

# A Novel Transformer-based Two Stage Framework for Multi-Label Image Classification

Zhi-Jie Wang  
College of Computer Science  
Chongqing University  
Chongqing, China  
cszjwang@cqu.edu.cn

Naikang Zhong\*  
Shanghai Intell. Edu. Big Data  
Eng. Tech. Res. Center  
Shanghai Normal University  
Shanghai, China  
1000465905@smail.shnu.edu.cn

Xiao Lin\*  
Shanghai Intell. Edu. Big Data  
Eng. Tech. Res. Center  
Shanghai Normal University  
Shanghai, China  
lin6008@shnu.edu.cn

**Abstract**—Multi-label image classification (MLIC) has received much attention due to its wide applications. Recently, the Transformer-based methods have exhibited excellent performance on MLIC tasks. Existing Transformer-based methods either used standard encoders that employ traditional relative positional encoding, or discarded encoders by focusing on the decoders to establish relations between labels and the regions of interest (RoI) in images. Yet, they pay less attention on enhancing the encoders. Moreover, the self-attention layer in the decoder is often employed in existing works, and is considered a component that could potentially enhance the internal relationships of label embeddings. It yet is unclear whether the self-attention layer is really helpful in establishing label correlation. Last but not least, existing Transformer-based methods use Asymmetric Loss to alleviate the sample imbalance problem; however, Asymmetric Loss may lead to the exclusion of some negative samples that are actually helpful for model training. To address these issues, this paper presents a novel Transformer-based two stage framework, which can be viewed as a fusion of the RoI based technique and an adapted Transformer. Our framework captures global and local features in model training. It is simple and easy-to-implement, but can achieve excellent performance. We have conducted extensive experiments on two widely used public datasets. The results consistently show us that our proposed method is feasible and also competitive, compared against state-of-the-art models.

**Index Terms**—Transformer, multi-label image classification, deep learning.

## I. INTRODUCTION

Image classification (1; 2; 3) is to analyze input images and categorize them into predefined classes based on their content. Specifically, the objective of image classification is to assign one or more category labels to an image according to the objects, scenes, or other features. Image classification can be viewed as a branch of data classification, it has been extensively studied in data mining and computer vision community (4; 5; 6; 7; 8). With the rapid development of deep learning, image classification tasks have achieved significant advancements and are now widely used in various real-world domains, such as image retrieval (9), object detection(10), image segmentation (11), and image processing (12).

Image classification contains two types of cases: single-label image classification (SLIC) (13; 14) and multi-label image

classification (MLIC) (14; 15; 16; 17; 18; 19). SLIC refers to the task of assigning an image to a single category or label. In this type of task, the image is assigned to only one most relevant label. In contrast, MLIC often assigns an image to multiple labels or categories. It is more challenging than SLIC due to various reasons (e.g., a greater variety of objects within the images).

Early methods for MLIC often transform it into single-label problem, and then use region of interest (RoI) based techniques (20; 21). Owing to the rapid advancement of convolutional neural networks (CNNs) and their excellent feature extraction capabilities, CNNs often utilizes convolutional layers to extract features from input images, and the resultant feature maps are utilized to predict and determine the presence of specific target categories. Some works have studied attention mechanisms (17; 22). Methods combining attention mechanisms with convolutional neural networks (CNNs) can further focus on more important local features. However, they often incur issues such as incomplete feature representation, insufficient utilization of inter-label correlations and dependencies, and relatively poor generalization ability. Later, with the rise of graph convolutional networks (GCNs), some researchers have focused on developing graph convolution based methods for multi-label image classification (1; 16). They can establish correlations and dependencies between labels, and exhibit strong generalization capabilities. However, these methods are computationally intensive, requiring substantial computational resources. Additionally, they carry a risk of overfitting in cases of unreasonable graph structures or significant noise.

Recently, Transformer-based framework has attracted much attention (3; 19; 22; 23). These approaches effectively integrate spatial information with semantic information. Particularly, it is much more flexible in modeling the relationship between image features and labels. These characters are beneficial to enhance the model’s classification performance and generalization capabilities. Yet, there remains several issues: (i) Existing works either used standard encoders that employ traditional relative positional encoding, or focused on leveraging the decoder to establish relations between labels and the RoI, i.e., depriving encoders directly. As for the former, traditional relative positional encoding is originally designed

\*Corresponding Author

for one dimensional sequence data, which might be improper for image data. As for the latter, the utility and effectiveness of the Transformer encoder is ignored, which might harm the performance. (ii) The self-attention layer in the decoder is often employed in existing works, and is considered a component that could potentially enhance the internal relationships of label embeddings. We realize that, in MLIC tasks, the input to the decoder consists of learnable label embeddings, where the labels themselves are not inherently correlated, since they are independent texts. If one conducts self-attention calculations on these learnable label embeddings, it actually forces the labels to learn relationships with each other; this may lead to spurious/fake label correlations. In other words, it is unclear whether the self-attention layer is really helpful in establishing label correlation. (iii) Existing Transformer-based methods use Asymmetric Loss to alleviate the problem of positive and negative sample imbalance; however, Asymmetric Loss mainly excludes easy negative samples through a hard threshold mechanism, which may lead to the exclusion of some negative samples that are actually helpful for model training.

To alleviate the above issues, we propose a new Transformer-based framework. It consists of four major components: (i) Feature extracting, which integrates data augmentation and CNNs together to extract local image features. (ii) Feature reshaping, which utilizes a  $1 \times 1$  convolution and learned positional encoding together to perform dimension reduction and features serialization. (iii) Feature label correlation, which uses an enhanced Transformer structure to learn global feature information, and performs cross-attention computations between learnable label embeddings and the globally extracted image features. (iv) Final classification and Loss, which obtains the classification score based on a linear projection layer and sigmoid function. To summarize, our main contributions can be listed as follows:

- We proposed a novel Transformer-based two stage framework. To our knowledge, for MLIC tasks, it is the first attempt to introduce image relative positional encoding (IRPE) into the Transformer encoder. Our method is simple, easy-to-implement but without loss of efficiency.
- We conducted extensive experiments on two widely-used datasets including MS-COCO and PASCAL VOC. The experimental results consistently show us that the proposed model can achieve competitive performance, compared against state-of-the-art models.

## II. RELATED WORK

In recent years, many methods have been proposed for MLIC. One type of approach is based on Region of Interest, another type of approach is based on Transformer. Our method combines these types of techniques, and thus is highly related to them. Next, we review previous works most relevant to ours.

### A. Regions of Interest

It is crucial to locate regions of interest (RoI) in computer vision tasks (19; 20; 21). Early methods for MLIC often transform it into single-label problem, and then use region

based techniques (20; 21). For example, Wei *et al.* (20) proposed a flexible deep CNN infrastructure to produce the multi-label predictions. Afterwards, many powerful region-based methods were developed (17; 19; 24). For example, Wang *et al.* (24) suggested to locate attentional regions by using a spatial transform layer. Recently, the work (22) defined spatial class-aware attention, which is used to reinforce the correct causal relationships. The afore-mentioned methods can efficiently focus on important local information, they however often suffer from incomplete feature representation and relatively weak ability to extract global features. To address this issue, researchers developed methods considering global and local features together (18; 25). Our method also considers both global and local features, but is different from theirs. In brief, our method enhances information interconnections among different regions, by introducing a two-dimensional relative positional encoding into Transformer encoders.

### B. Transformer

The Transformer (26) was initially been applied to natural language processing tasks. Recently, the Transformer architecture has been applied in computer vision. Particularly, many studies (3; 19; 22; 23) have employed Transformers for MLIC. Some works (3; 22) mainly utilized Transformer encoders to extract global image features. For example, Zhao *et al.* (3) used a Transformer encoder to capture contextual information. Nevertheless, these works often use standard Transformer encoders that employ traditional relative position encoding or do not employ relative position encoding at all. Unlike these works, our paper introduces the Image Relative Position Encoding (IRPE), which is specifically designed for 2D images, into the Transformer encoder. This idea addresses the shortcomings of traditional relative position encoding which is originally designed for language sequences.

Recently, some studies (19; 23) have focused on using Transformer decoders to establish relationships between labels and image features. For example, (19) used the cross-attention mechanism built in the Transformer decoder to establish relationships between labels and image features. Our work is most similar to (19), as our method bears many similarities with it (e.g., utilizing a Transformer decoder to query the presence of category label). However, these methods often overlook the importance of the Transformer encoder. Instead, we claim that the Transformer encoder is also useful, as it plays a crucial role in global information extraction and spatial structure modeling. Compared to (19), there are several obvious differences: (i) We use the Transformer encoders to help the model acquire global feature information, and we further employ IRPE to enhance the performance; (ii) We analyze the self-attention layers in the decoder, and point out that they are often unhelpful for MLIC tasks; and (iii) we introduced the Asymmetric Polynomial Loss which is not covered in their paper.

### C. Others

Previous works considered also label correlations (1; 6; 16). For example, Chen *et al.* (16) utilized graph convolutional

networks (GCNs) to construct directed graphs on labels. Ye *et al.* (1) proposed an attention-driven dynamic graph convolutional network. These methods establish correlations and dependencies between labels. They, however, often rely on graph structures that require substantial computational resources, and sometimes they may get false correlations, harming the performance (14; 19). In contrast, our method does not require the construction of complex graph models, it instead directly detects image regions relevant to categories.

Loss functions are also obviously important to classification quality. The binary cross-entropy loss can be used in multi-label image classification, but such a loss function often fails to address class imbalance issue, which is crucial for the model’s performance. To this, many works (2; 27; 28) have focused on improving loss functions. For example, Ridnik *et al.* introduced the asymmetric loss (2). Huang *et al.* (28) proposed the Asymmetric Polynomial Loss, which leverages asymmetric focusing mechanisms to alleviate the imbalance problem. Inspired by its excellent performance, our work adopts the Asymmetric Polynomial Loss.

### III. METHOD

In this section, we first present an overview of our proposed model, and then cover the details of the model.

#### A. Overview of Our Model

Fig. 1 illustrates the architecture of our model. The first step is feature extraction. Specifically, for a given input image, we first apply data augmentation and then feed it into a convolutional-based model to extract preliminary image features. The second stage is feature reshaping. Generally speaking, for the preliminary image feature, we first conduct the dimensionality reduction by using a 1x1 convolution, and then combine it with the learned positional embedding, by executing a “+” operator between feature vectors. Afterwards, we obtain the serialized feature information by “flattening” the combined feature vectors. Later, the serialized feature information is to be passed into the next stage. The third stage is feature label interaction. The essence of this step is to extract global image features and to locate regions of interest according to specific categories. More specifically, in this stage, we develop a variant of the standard Transformer structure. In our structure, we introduce IRPE into the encoder, which is beneficial to capture richer global features. Meanwhile, in the decoder part, we, based on empirical study, remove the self-attention layer that was used in prior studies. The final stage is to obtain multi-label prediction scores. Specifically, the feature vectors from the decoder are to be transformed into logits via a linear projection layer, the multi-label prediction scores can be obtained by the sigmoid function.

#### B. Feature Extracting and Reshaping

To better understand this stage, we first introduce the concepts of Cutout and learned positional encoding.

1) *Cutout*: Cutout is a data augmentation technique involving the following two steps: (i) Random Region Selection. Randomly select a rectangular region within the image. (ii) Masking the Region. Set the pixel values in the selected rectangular region to zero or apply random noise. This masks the chosen region within the image. The resulting image with the masked region serves as a new training sample, contributing to increasing data diversity and model robustness, ultimately improving generalization.

2) *Learned positional encoding*: The learned positional encoding is actually a technique for modeling positional information in deep learning models. Unlike traditional absolute positional encodings based on sine and cosine functions, the learned positional encoding does not rely on a predefined mapping from positions to vectors, it can be implemented with a simple embedding layer. During model training, the weights of these embedding layers are adjusted to minimize task-specific loss functions, enabling the model to learn optimal positional representations. In other words, it learns the vector representation for each position during training, providing the model with more flexible and adaptive positional information.

With the above concepts in mind, we proceed to explain the details of “Feature Extracting and Reshaping”. Given an image  $x \in \mathbb{R}^{H \times W \times 3}$  as an input, we first implement the Cutout, and then extract local spatial feature  $F \in \mathbb{R}^{H' \times W' \times d_0}$  using CNN-based backbone models (e.g., ResNet, TresNet, ConvNext), where  $H$  and  $W$  respectively denote the height and weights of the original image,  $H'$  and  $W'$  respectively denote the height and weights of the feature map  $F$ , and  $d_0$  represents the dimensionality of feature map  $F$ . Next, we reshape the features to match the input expected by the Transformer. Specifically, we divide the reshaping into two steps:

(i) *Dimension Reduction to Hidden Dimension*: We perform this using a 1x1 convolution to transform the features from  $H' \times W' \times d_0$  to  $H' \times W' \times d_{model}$ , where  $d_{model}$  is the desired hidden dimension. This can be achieved as follows:

$$Y = \text{Conv}_{1 \times 1}(F), \quad Y \in \mathbb{R}^{H' \times W' \times d_{model}} \quad (1)$$

where,  $\text{Conv}_{1 \times 1}$  denotes the 1x1 convolution operation, converting  $d_0$  channel feature maps into  $d_{model}$  ones.

(ii) *Flattening into Sequence Data*: The reduced features  $Y$  are reshaped from a 3D tensor ( $H' \times W' \times d_{model}$ ) into a 2D tensor representing a sequence of data, with dimensions  $d_{model} \times L$ , where  $L = H' \times W'$  is the sequence length. This can be implemented with the following formula:

$$Z = \text{Reshape}(Y), \quad Z \in \mathbb{R}^{d_{model} \times L} \quad (2)$$

where  $Z$  represents the reshaped sequence features, Reshape involves the Flatten operation followed by transposition of certain dimensions.

#### C. Feature-Label Interaction

There are two major components: the enhanced encoder and decoder, respectively (recall Fig. 1). The core element of our enhanced encoder is the self-attention mechanism that

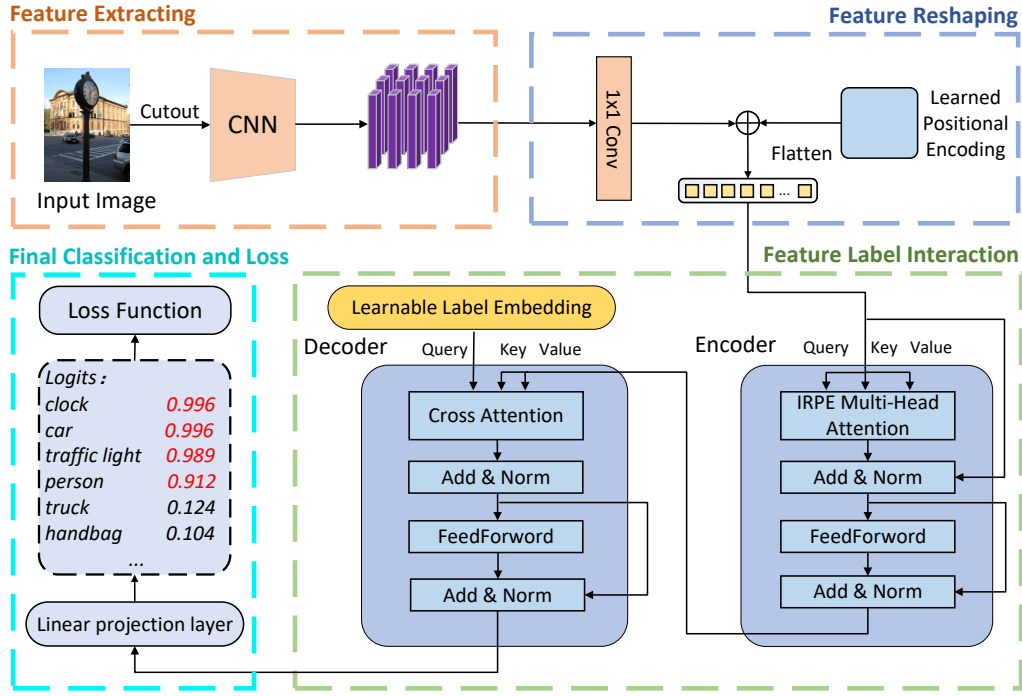


Fig. 1: The architecture of our model.

incorporates IRPE. This mechanism aims to provide directional information for the sequential image features in a two-dimensional encoding, enabling the model to extract better global features. The core element of the enhanced decoder is the cross-attention mechanism. We use learnable label embeddings as queries and the global image features obtained from the encoder as keys and values for cross-attention calculation. Next, we first cover the details of IRPE, and then discuss the enhanced encoder and decoder, respectively.

1) *Image Relative Positional Encoding*: Inspired by (29), we attempt to incorporate IRPE into our model. One can incorporate the dot-product and context based IRPE. To understand how IRPE is incorporated into the encoder, we briefly introduce the process of applying IRPE simultaneously to query, key, and value, for example. First, we can apply IRPE to both query and key. The dot-product attention weights  $e_{ij}$  is computed as:

$$e_{ij} = \frac{(x_i W^Q) (x_j W^K)^T + b_{ij}}{\sqrt{d_z}} \quad (3)$$

where  $b_{ij} \in \mathbb{R}$  is the 2D relative positional encoding. For the contextual mode,

$$b_{ij} = (x_i W^Q) (r_{ij}^K)^T + (x_j W^K) (r_{ij}^Q)^T \quad (4)$$

where  $r_{ij}^K, r_{ij}^Q \in \mathbb{R}^d$  are both learnable vectors. Second, we incorporate IRPE into the value. Consequently, the output after the self-attention layer can be represented as:

$$z_i = \sum_{j=1}^n \text{softmax}(e_{ij}) (x_j W^V + r_{ij}^V) \quad (5)$$

2) *Encoder*: Recall Section III-B, we have obtained local image features. To obtain the global features, we need to perform a second round of feature extraction on the feature maps. We achieve it by using the self-attention mechanism within the Transformer. Specifically, the reshaped serialized image features undergo a linear transformation to map them into q, k, and v inputs for the self-attention layer. By combining the self-attention layer with the applied IRPE, we capture more comprehensive global image features. The self-attention layers in the enhanced encoder enable each image feature vector to interact with all other feature vectors, facilitating the global contextual information. Formally, the computational process of the self-attention layer is as follows:

$$F_i = \text{MultiHead}(Z_i, \tilde{Z}_i, Z_i) \quad (6)$$

where  $Z_i$  represents image sequence feature,  $\tilde{Z}_i$  represents image sequence feature augmented with image relative positional encoding,  $F_i$  represents the new feature representation obtained from image sequences after undergoing multi-head attention.

3) *Decoder*: We utilize learnable label embeddings as queries, image features from the encoder as keys and values; and we employ multi-layer Transformer decoders to perform cross-attention computation, aiming to identify regions of interest. Specifically, the cross-attention computation is:

$$Q_j = \text{MultiHead}(Q_{j-1}, F_i, F_i) \quad (7)$$

where  $Q_j$  denotes the query input; when  $j = 1$ ,  $Q_0$  represents the learnable label embedding;  $F_i$  denotes the sequence of

image features obtained from the encoder, and it is actually identical to the  $F_i$  in Equation 6.

Note that the decoder structure we used excludes the self-attention layer. In prior studies, the self-attention layer within the decoder was considered a component that could potentially enhance the internal relationships of label embeddings. However, we realize that, in multi-label image classification tasks, the input to the decoder consists of learnable label embeddings, where the labels themselves are not inherently correlated, since they are independent texts. If one conducts self-attention calculations on these learnable label embeddings, it actually forces the labels to learn relationships with each other, potentially leading to spurious/fake label correlations.

#### D. Final Classification and Loss

1) *Final Classification*: After the feature-label interaction is completed, we use a linear projection layer to assign a corresponding value to each class, and obtain the corresponding prediction score using a sigmoid function.

2) *Loss*: To address the issue of sample imbalance, our framework generally employs an asymmetric polynomial loss (APL) function, although traditional binary cross-entropy and focal loss can also be utilized. Here, APL is built upon the foundation of asymmetric loss, it employs a Taylor expansion to enable the function to fit more complex computations. The specific computation is detailed as follows:

$$L_{APL} = \sum_{i=0}^C \left\{ y_i(1-p_i)^{\gamma^+} \left[ -\log p_i + (\alpha_1 - 1)(1-p_i) + \left( \alpha_2 - \frac{1}{2} \right) (1-p_i)^2 \right] + (1-y_i)p_{res}^{\gamma^-} \left[ -\log(1-p_i) + (\beta_1 - 1)p_{res} \right] \right\} / C \quad (8)$$

where  $y_i$  represents the true label of the  $i$ th sample,  $p_i$  represents the predicted probability of the  $i$ th sample being in the positive class,  $C$  are coefficients, and  $p_{res}$  denotes  $\max(p_i - p_{th}, 0)$ . In our experiments, we set  $\gamma^+ = 0$  and  $\gamma^- = 2$  by default.

## IV. EXPERIMENTS

### A. Datasets, Evaluation Metrics, and Competitors

To assess our method, we conducted experiments on two datasets, namely, MS-COCO (33) and PASCAL VOC (34).

- **MS-COCO<sup>1</sup>**: It is a large-scale dataset designed for object detection and segmentation, widely used in recent years for evaluating multi-label image classification. It comprises 82,783 training images, 40,504 validation images, covering 80 common objects, with an average of 2.9 labels per image.

- **PASCAL VOC<sup>2</sup>**: It contains two versions: VOC 2007 and VOC 2012. VOC 2007 is utilized for object detection and image classification tasks. This dataset comprises 5011 images

as the *train-val* set and 4952 images as the *test* set, covering 20 common object categories. The object categories within VOC 2007 encompass humans, dogs, cats, airplanes, ships, bicycles, and more. Each object instance is annotated with its corresponding category label and bounding box delineating its spatial extent. VOC 2012 is a classic dataset used for object detection and image segmentation tasks. It comprises bounding boxes for each object and pixel-level segmentation annotations. VOC 2012 consists of 11,540 images for the *train-val* set and 10,991 images for the *test* set.

In terms of evaluation metrics, we utilized the Average Precision (AP) for each individual class; and we use the mean Average Precision (mAP) across all classes, which is computed as follows:  $mAP = \frac{\sum_{c=1}^C AP_c}{C}$ , where  $c$ , and  $C$  denote current specific class, and number of all classes respectively. Meanwhile, we employed Overall Precision (OP), Overall Recall (OR), and Overall F1-Score (OF1), they are computed as:  $OP = \frac{\sum_i M_c^i}{\sum_i M_p^i}$ ,  $OR = \frac{\sum_i M_c^i}{\sum_i M_g^i}$ ,  $OF1 = \frac{2 \times OP \times OR}{OP + OR}$ . Also, we utilized per-Category Precision (CP), per-Category Recall (CR), and per-Category F1-Score (CF1), they are computed as:  $CP = \frac{1}{C} \sum_i \frac{M_c^i}{M_p^i}$ ,  $CR = \frac{1}{C} \sum_i \frac{M_c^i}{M_g^i}$ ,  $CF1 = \frac{2 \times CP \times CR}{CP + CR}$ .

To examine the competitiveness of our proposed method, we compared it with state-of-the-art methods (e.g., published in ICLR 2023 (22) and CVPR 2023 (31)). These competitors can be categorized into three classes (recall Section II):

- **Region of Interest based methods**: ResNet101 (13), Fev+lv (21), HCP (20), RDAL (24), MCAR (18), TResNetL (35), Convnextv2-B (31), Swin-L (32).
- **Transformer-based methods**: TDRG (3), IDA (22), Q2L (19), C-Trans (30).
- **Other methods**: CNN-RNN (6), SRN (15), ML-GCN (16), MS-CMA (17), CCD (14), SSGRL (36), ADD-GCN (1).

### B. Experimental Settings

We adopted the following settings by default, unless stated otherwise. As for the image enhancement, we used cutout; and for regularization we used RandAugment. Considering GPU efficiency and ensuring fairness and convenience, we selected ResNet101, Tresnet-L, and Convnextv2-Base as the backbone models when comparing various methods. Regarding resolution, we utilized three resolutions: 384, 448, and 576. In what follows, when we use ResNet101 and 448 resolution, the resulting output features of backbone are denoted as  $H \times W \times d_0 = 14 \times 14 \times 2048$ . Subsequently, the obtained image features are reshaped to match the shape required by the Transformer. Specifically, in our experiments, we employed one encoder layer and two decoder layers (which can be adjustable as needed) to update the label features. Finally, we accomplished the classification via a linear projection layer.

We trained the model for 80 epochs using an AdamW optimizer with a weight decay of 5e-3, a momentum of 0.9;  $\beta_1$  and  $\beta_2$  are set to 0.9 and 0.9999, respectively. Additionally, we employed the one-cycle learning rate policy with a maximum learning rate of 5e-5. The experimental platform is

<sup>1</sup><https://cocodataset.org>

<sup>2</sup><http://host.robots.ox.ac.uk/pascal/VOC/>

TABLE I: Comparison results on the MS-COCO dataset. The backbones marked with 22k are pre-trained on the ImageNet-22k dataset. In the comparison, our primary focus lies in assessing more comprehensive metrics, including mAP, CF1, and OF1. Other metrics can be used for reference.

Method	Backbone	Resolution	mAP	CP	CR	CF1	OP	OR	OF1
SRN(15)	ResNet101	224x224	77.1	81.6	65.4	71.2	82.7	69.9	75.8
ResNet-101(13)	ResNet101	224x224	78.3	80.2	66.7	72.8	83.9	70.8	76.8
ML-GCN(16)	ResNet101	448x448	83.0	85.1	72.0	78.0	85.8	75.4	80.3
MS-CMA(17)	ResNet101	448x448	83.8	82.9	84.4	78.4	84.4	77.9	81.0
MCAR(18)	ResNet101	448x448	83.8	85.0	72.1	78.0	88.0	73.9	80.3
Q2L(19)	ResNet101	448x448	84.9	84.8	74.5	79.3	86.6	76.9	81.5
SSGRL(7)	ResNet101	576x576	83.8	89.9	68.5	76.8	91.3	70.8	79.7
C-Trans(30)	ResNet101	576x576	85.1	86.3	74.3	79.9	87.7	76.5	81.7
ADD-GCN(1)	ResNet101	576x576	85.2	84.7	75.9	80.1	84.9	79.4	82.0
TDRG(3)	ResNet101	576x576	86.0	87.0	74.7	80.4	87.5	77.9	82.4
IDA(22)	ResNet101	576x576	86.3	-	-	80.4	-	-	82.5
Q2L(19)	ResNet101	576x576	86.5	85.8	76.7	81.0	87.0	78.9	82.8
Ours	ResNet101	448x448	85.2	84.9	74.7	79.5	86.8	76.9	81.5
Ours	ResNet101	576x576	<b>86.8</b>	85.9	77.0	<b>81.2</b>	87.3	79.0	<b>83.0</b>
Convnextv2-B(31)	ConvNextv2-B(22k)	384x384	89.6	89.3	80.5	84.7	89.5	82.1	85.7
Swin-L(32)	Swin-L(22k)	384x384	89.6	89.9	80.2	84.8	90.4	82.1	86.1
CCD(14)	Swin-L(22k)	384x384	90.3	85.9	84.0	84.6	85.1	86.4	85.7
Ours	ConvNextv2-B(22k)	384x384	<b>91.1</b>	89.8	82.3	<b>85.9</b>	90.0	83.8	<b>86.8</b>

an Ubuntu 18.04 system, equipped with an Intel Xeon Gold 6330 processor @ 2.0 GHz with 60 cores, 240 GB of RAM, and 6 Nvidia GeForce RTX 3090 GPUs.

### C. Comparison with State-Of-The-Art Methods

1) *Performance on MS-COCO*: Table I presents the comparative results. We can see that, when Resnet-101 is used as the backbone, our model consistently outperforms other state-of-the-art methods in terms of mAP, CF1, OF1, and some other reference metrics. Particularly, although Q2L also employs a Transformer based two-stage approach, our model beats it in all metrics at both resolutions. Also, our model beats the IDA(22) (ICLR’2023) by 0.5% at 576X576 resolution. Remark that, an increase of 0.5% is non-trivial in MLIC tasks. All these results consistently demonstrate the competitiveness and effectiveness of our proposed approach.

Furthermore, we have observed that our proposed framework is highly compatible with the ConvNeXt V2 backbone. The unique Global Response Normalization (GRN) layer of ConvNeXt V2 effectively addresses the issue of feature collapse, preventing label embeddings from activating similar but incorrect image regions, thereby enhancing the model’s comprehension of input data. ConvNeXt V2 is adept at extracting rich local features while avoiding redundant activations across different feature channels. Meanwhile, the Transformer component focuses on processing global features and precise activation of label-specific features. Particularly, after the incorporation of the IRPE, the Transformer encoder in conjunction with the ConvNeXt V2 can leverage the best global feature extraction capabilities, thereby improving the model’s accuracy. Experimental results indicate that our method can beat the baseline (ConvNeXt V2-Base) by 1.5%, achieving an ultra-high precision of 91.1% on the MS-COCO dataset. This validates the effectiveness of integrating our framework and ConvNeXt V2. We have to mention that, it is non-trivial

to obtain an increase of 1.5% to the competitor, Convnext2-B (31), published in 2023.

2) *Performance on PASCAL VOC*: (i) Results on VOC 07. Table II presents the results. In the first part of Table II, we utilized the standard Resnet101 as the backbone with a 448 resolution. The reported metrics include the AP values of 20 categories and the overall mAP. We can see that our method achieves the best results in most categories. In terms of mAP, we have surpassed all these methods. More specifically, comparing to region-based approaches (e.g., Fev+Lv, HCP, RDAL), it can be observed that our result is obviously better than them. This is mainly because our method utilizes the Transformer decoder to obtain class-specific representations, resulting in more accurate ROI (i.e., region of interest). On the other hand, our method also beats the Transformer-based methods (e.g., TDRG), this is mainly because our method introduces IRPE into the encoder, providing us the spatial relationships between pixels. In the second part of Table II, except for SSGRL and ADD-GCN, which use Resnet101, all other methods use Tresnet-L. We can see that our model also achieves the best results in most categories. Particularly, we achieved a mAP value of 96.2% on this dataset. Considering the experimental results in Table II as a whole, our method beats all these competitors in terms of mAP.

(ii) Results on VOC 12. Since complete labels for the *test* set are not provided officially, we conducted testing on the official evaluation server. Table III presents the comparative results (the reader can also visit the anonymous link<sup>3</sup>). The training strategy used in this experiment is the same as that for the second part of VOC 2007. Similar to the results demonstrated on the VOC 2007 dataset, we also achieved the state-of-the-art performance on the VOC 2012 dataset. Particularly, we observe that, even if SSGRL and ADDGCN used a higher resolution (576x576), we still achieve higher mAP values than theirs (i.e., demonstrating the competitiveness of our

<sup>3</sup><http://host.robots.ox.ac.uk:8080/anonymous/XFI9GJ.html>

TABLE II: Comparison results on PASCAL VOC 2007, in terms of AP and mAP in percentages. The resolution of all results are 448x448, with the exception of ADD-GCN and SSGRL, which have resolution of 576x576.

Methods	aero	bike	bird	boat	bottle	bus	car	cat	chair	cow	table	dog	horse	mbike	person	plant	sheep	sofa	train	tv	mAP
CNN-RNN(6)	96.7	83.1	94.2	92.8	61.2	82.1	89.1	94.2	64.2	83.6	70.0	92.4	91.7	84.2	93.7	59.8	93.2	75.3	<b>99.7</b>	78.6	84.0
Fev+Lv(21)	97.9	97.0	96.6	94.6	73.6	93.9	96.5	95.5	73.7	90.3	82.8	95.4	97.7	95.9	98.6	77.6	88.7	78.0	98.3	89.0	90.6
HCP(20)	98.6	97.1	98.0	95.6	75.3	94.7	95.8	97.3	73.1	90.2	80.0	97.3	96.1	94.9	96.3	78.3	94.7	76.2	97.9	91.5	90.9
RDAL(24)	98.6	97.4	96.3	96.2	75.2	92.4	96.5	97.1	76.5	92.0	87.7	96.8	97.5	93.8	98.5	81.6	93.7	82.8	98.6	89.3	91.9
MCAR(18)	99.7	99.0	98.5	98.2	<b>85.4</b>	96.9	97.4	<b>98.9</b>	83.7	95.5	88.8	<b>99.1</b>	98.2	95.1	99.1	84.8	97.1	<b>87.8</b>	98.3	94.8	94.8
TDRG(3)	<b>99.9</b>	98.9	98.4	<b>98.7</b>	81.9	95.8	97.8	98.0	<b>85.2</b>	95.6	<b>89.5</b>	98.8	98.6	97.1	99.1	86.2	97.7	87.2	99.1	<b>95.3</b>	95.0
Ours	<b>99.9</b>	<b>99.3</b>	<b>98.9</b>	<b>98.1</b>	84.8	<b>97.6</b>	<b>98.6</b>	<b>98.9</b>	82.7	<b>98.3</b>	88.0	98.8	<b>98.7</b>	<b>97.3</b>	<b>99.2</b>	<b>88.8</b>	<b>98.6</b>	85.3	99.4	94.9	<b>95.3</b>
SSGRL(7)	99.7	98.4	98.0	97.6	85.7	96.2	98.2	98.8	82.0	98.1	89.7	98.8	98.7	97.0	99.0	86.9	98.1	85.8	99.0	93.7	95.0
ADD-GCN(1)	99.8	99.0	98.4	<b>99.0</b>	86.7	98.1	98.5	98.3	<b>85.8</b>	98.3	88.9	98.8	99.0	97.4	99.2	88.3	98.7	<b>90.7</b>	99.5	<b>97.0</b>	96.0
TResNet(35)	<b>99.9</b>	98.4	98.9	98.7	86.8	98.2	98.7	98.5	83.1	98.3	89.5	98.8	<b>99.2</b>	98.6	99.3	89.5	99.4	86.8	99.6	95.2	95.8
Q2L(19)	<b>99.9</b>	98.9	99.0	98.4	87.7	<b>98.6</b>	<b>98.8</b>	99.1	84.5	98.3	89.2	<b>99.2</b>	<b>99.2</b>	99.3	99.3	90.2	98.8	88.3	99.5	95.5	96.1
Ours	<b>99.9</b>	<b>99.1</b>	<b>99.2</b>	98.8	<b>87.9</b>	<b>98.6</b>	98.7	<b>99.2</b>	83.4	<b>98.4</b>	<b>90.6</b>	99.1	98.9	98.9	<b>99.4</b>	<b>90.5</b>	<b>99.7</b>	88.6	<b>99.8</b>	95.7	<b>96.2</b>

TABLE III: Comparison results on PASCAL VOC 2012. The resolution of all results are 448x448, except that ADD-GCN and SSGRL have resolution of 576x576. Differing from the VOC2007 dataset, for the sake of impartiality, we conducted tests utilizing the official evaluation server, all results obtained are provided by the VOC2012 official evaluation server.

Methods	aero	bike	bird	boat	bottle	bus	car	cat	chair	cow	table	dog	horse	mbike	person	plant	sheep	sofa	train	tv	mAP
Fev+Lv(21)	98.4	92.8	93.4	90.7	74.9	93.2	90.2	96.1	78.2	89.8	80.6	95.7	96.1	95.3	97.5	73.1	91.2	75.4	97.0	88.2	89.4
HCP(20)	99.1	92.8	97.4	94.4	79.9	93.6	89.8	98.2	78.2	94.9	79.8	97.8	97.0	93.8	96.4	74.3	94.7	71.9	96.7	88.6	90.5
MCAR(18)	99.6	97.1	98.3	96.6	87.0	95.5	94.4	98.8	87.0	96.9	85.0	98.7	98.3	97.3	99.0	83.8	96.8	83.7	98.3	93.5	94.3
SSGRL(7)	99.7	96.1	97.7	96.5	86.9	95.8	95.0	98.9	88.3	97.6	87.4	99.1	99.2	97.3	99.0	84.8	98.3	85.8	99.2	94.1	94.8
ADD-GCN(1)	99.8	97.1	98.6	96.8	89.4	97.1	96.5	99.3	89.0	97.7	87.5	99.2	99.1	97.7	99.1	86.3	<b>98.8</b>	87.0	99.3	95.4	95.5
CCD(14)	99.8	98.2	98.3	98.0	88.6	97.4	96.9	99.1	90.8	<b>98.9</b>	<b>90.2</b>	99.2	<b>99.6</b>	98.4	99.0	87.7	98.4	88.8	99.7	96.4	96.1
Q2L(19)	99.9	98.2	<b>99.3</b>	98.1	90.4	<b>97.7</b>	97.4	99.4	<b>92.7</b>	98.7	89.9	<b>99.4</b>	99.5	<b>99.0</b>	<b>99.4</b>	88.4	<b>98.8</b>	89.3	99.6	96.8	96.6
Ours	<b>100.0</b>	<b>98.5</b>	99.1	<b>98.5</b>	<b>90.6</b>	97.5	<b>97.6</b>	<b>99.5</b>	91.8	98.6	89.6	<b>99.4</b>	99.3	98.9	<b>99.4</b>	<b>89.2</b>	98.7	<b>90.5</b>	<b>99.8</b>	<b>97.0</b>	<b>96.7</b>

TABLE IV: Comparisons of our encoders, standard encoders, and no encoders. Our encoder contains IRPE. The resolution of 448x448 is utilized.

Setting	mAP
w/ our encoder	<b>85.22</b>
w/ standard encoder	84.90
w/o encoder	84.72

model). The possible reasons are that, SSGRL and ADD-GCN used graph structures to establish label correlations, primarily focusing on local features, their ability to capture global features is weak. In contrast, our method utilized cross-attention to compute the attention weights of each label for different image regions, it implicitly captured the relationships between labels; furthermore, our encoder with IRPE can acquire global information efficiently.

#### D. Ablation study

1) *Encoder*: Previous works based on the Transformer architecture either overlook the importance of the encoder, or only use standard encoders. Table IV confirms the necessity of the encoder in multi-label image classification model. We can see that, on the MS-COCO dataset, employing a standard Transformer yields a performance increase, compared to the Transformer without encoders. Particularly, when our enhanced encoder is employed, the performance is enhanced further.

2) *Self-Attention*: The self-attention layer in the Transformer decoder is often thought to enable better embedding representations of labels, and previous works that used the standard decoder often employ the self-attention layer. In Section III-C3, we argue that the self-attention layer in the decoder may be not much helpful. To validate this, we conducted experiments on the MS-COCO dataset. Table V shows

TABLE V: Comparison results between using self-attention layers and without self-attention layers. "\*" denotes that self-attention layer is only used in the second decoder.

Setting	mAP
w/ self-attention	85.14
w/ self-attention*	85.07
w/o self-attention	<b>85.20</b>

TABLE VI: Comparison between different loss functions.

Loss Function	mAP
Binary Cross-Entropy	84.92
Focal Loss(27)	85.11
Asymmetric Loss(2)	85.15
Asymmetric Polynomial Loss(28)	<b>85.20</b>

the results. From this table, we can see that removing self-attention layers from the decoder achieves better performance. One of possible reasons is that, applying self-attention to these learnable label embeddings forces the labels to learn inter-relationships, which may result in spurious label correlations, as mentioned in Section III-C3. Another possible reason is that, before computing cross-attention (recall Fig. 1), the input label embeddings undergo a linear transformation, which enables the input to fit adaptively the cross-attention module's expected input; in other words, removing self-attention layer in decoders makes less or even no negative impact.

3) *Loss Function*: The Asymmetric Polynomial Loss (APL) utilizes a Taylor expansion relative to the Asymmetric Loss (AL), allowing it to handle more intricate computations. On the other hand, compared to Binary Cross-Entropy (BCE) and Focal Loss (FL), it possesses better capabilities in addressing sample imbalance issues. To validate their performance when they are integrated into our framework, we conducted comparisons. For Asymmetric Loss and Asymmetric Polyno-

mial Loss, we configured  $\gamma+ = 0$  and  $\gamma- = 2$  respectively. The experimental results are shown in Table VI. We can see that the best performance is achieved when loss function is Asymmetric Polynomial Loss. The reason could be that, APL can provide a more refined ability of handling positive and negative samples than other competitors.

## V. CONCLUSION

In this paper, we have proposed a novel framework for multi-label image classification. Our framework incorporates RoI-based technique and an enhanced Transformer structure. We have validated its competitiveness on several widely used multi-label image classification datasets. Our study yields several important findings for MLIC tasks: (i) incorporating IRPE into Transformer decoders is useful; (ii) removing self-attention layers in the Transformer decoder has no negative impact, or even improves the performance; and (iii) the APL function could be more compatible with Transformer-based frameworks, compared against BCE, FL, and AL.

## ACKNOWLEDGMENT

This work was supported by the National Natural Science Foundation of China (No.61972425, 62477013) and Shanghai Municipal Science and Technology Commission's 2024 Science Popularization Special Project(24DZ2305900).

## REFERENCES

- [1] J. Ye, J. He, X. Peng, W. Wu, and Y. Qiao, "Attention-driven dynamic graph convolutional network for multi-label image recognition," in *Proceedings of ECCV*, pp. 649–665, 2020.
- [2] T. Ridnik, E. Ben-Baruch, N. Zamir, A. Noy, I. Friedman, M. Protter, and L. Zelnik-Manor, "Asymmetric loss for multi-label classification," in *Proceedings of ICCV*, pp. 82–91, 2021.
- [3] J. Zhao, K. Yan, Y. Zhao, X. Guo, F. Huang, and J. Li, "Transformer-based dual relation graph for multi-label image recognition," in *Proceedings of ICCV*, pp. 163–172, 2021.
- [4] D. Rymarczyk, Ł. Struski, J. Tabor, and B. Zieliński, "Protopshare: Prototypical parts sharing for similarity discovery in interpretable image classification," in *Proceedings of SIGKDD*, pp. 1420–1430, 2021.
- [5] Z. Wang, M. Nie, K. Zhao, Z. Quan, and B. Yao, "Cover trees revisited: Exploiting unused distance and direction information," *IEEE Trans. Knowl. Data Eng.*, vol. 35, no. 11, pp. 11231–11245, 2023.
- [6] J. Wang, Y. Yang, J. Mao, Z. Huang, C. Huang, and W. Xu, "Cnn-rnn: A unified framework for multi-label image classification," in *Proceedings of CVPR*, pp. 2285–2294, 2016.
- [7] T. Chen, M. Xu, X. Hui, H. Wu, and L. Lin, "Learning semantic-specific graph representation for multi-label image recognition," in *Proceedings of ICCV*, pp. 522–531, 2019.
- [8] Z. Wang, D. Wang, B. Yao, and M. Guo, "Probabilistic range query over uncertain moving objects in constrained two-dimensional space," *IEEE Trans. Knowl. Data Eng.*, vol. 27, no. 3, pp. 866–879, 2015.
- [9] M. Zeng, B. Yao, Z.-J. Wang, Y. Shen, F. Li, J. Zhang, H. Lin, and M. Guo, "Catiri: An efficient method for content-and-text based image retrieval," *Journal of Computer Science and Technology*, vol. 34, pp. 287–304, 2019.
- [10] X. Lin, Z.-J. Wang, L. Ma, R. Li, and M.-E. Fang, "Salient object detection based on multiscale segmentation and fuzzy broad learning," *The Computer Journal*, vol. 65, no. 4, pp. 1006–1019, 2022.
- [11] T. Weng, Y. Shen, K. Jin, Y. Wang, Z. Cheng, Y. Li, G. Zhang, and S. Wang, "Enhancing point annotations with superpixel and confident learning guided for improving semi-supervised oct fluid segmentation," *Biomedical Signal Processing and Control*, vol. 94, p. 106283, 2024.
- [12] X. Lin, L. Ma, B. Sheng, Z.-J. Wang, and W. Chen, "Utilizing two-phase processing with fbls for single image deraining," *IEEE Transactions on Multimedia*, vol. 23, pp. 664–676, 2020.
- [13] K. He, X. Zhang, S. Ren, and J. Sun, "Deep residual learning for image recognition," in *Proceedings of CVPR*, pp. 770–778, 2016.
- [14] R. Liu, H. Liu, G. Li, H. Hou, T. Yu, and T. Yang, "Contextual debiasing for visual recognition with causal mechanisms," in *Proceedings of CVPR*, pp. 12755–12765, 2022.
- [15] F. Zhu, H. Li, W. Ouyang, N. Yu, and X. Wang, "Learning spatial regularization with image-level supervisions for multi-label image classification," in *Proceedings of CVPR*, pp. 5513–5522, 2017.
- [16] Z.-M. Chen, X.-S. Wei, P. Wang, and Y. Guo, "Multi-label image recognition with graph convolutional networks," in *Proceedings of CVPR*, pp. 5177–5186, 2019.
- [17] R. You, Z. Guo, L. Cui, X. Long, Y. Bao, and S. Wen, "Cross-modality attention with semantic graph embedding for multi-label classification," in *Proceedings of AAAI*, pp. 12709–12716, 2020.
- [18] B.-B. Gao and H.-Y. Zhou, "Learning to discover multi-class attentional regions for multi-label image recognition," *IEEE Transactions on Image Processing*, vol. 30, pp. 5920–5932, 2021.
- [19] S. Liu, L. Zhang, X. Yang, H. Su, and J. Zhu, "Query2label: A simple transformer way to multi-label classification," *arXiv preprint arXiv:2107.10834*, 2021.
- [20] Y. Wei, W. Xia, M. Lin, J. Huang, B. Ni, J. Dong, Y. Zhao, and S. Yan, "Hcp: A flexible cnn framework for multi-label image classification," *IEEE Transactions on Pattern Analysis and Machine Intelligence*, vol. 38, no. 9, pp. 1901–1907, 2015.
- [21] H. Yang, J. Tianyi Zhou, Y. Zhang, B.-B. Gao, J. Wu, and J. Cai, "Exploit bounding box annotations for multi-label object recognition," in *Proceedings of CVPR*, pp. 280–288, 2016.
- [22] R. Liu, J. Huang, T. H. Li, and G. Li, "Causality compensated attention for contextual biased visual recognition," in *Proceedings of ICLR*, 2023.
- [23] T. Ridnik, G. Sharir, A. Ben-Cohen, E. Ben-Baruch, and A. Noy, "ML-decoder: Scalable and versatile classification head," in *Proceedings of WACV*, pp. 32–41, 2023.
- [24] Z. Wang, T. Chen, G. Li, R. Xu, and L. Lin, "Multi-label image recognition by recurrently discovering attentional regions," in *Proceedings of ICCV*, pp. 464–472, 2017.
- [25] J. Zhan, J. Liu, W. Tang, G. Jiang, X. Wang, B.-B. Gao, T. Zhang, W. Wu, W. Zhang, C. Wang, *et al.*, "Global meets local: Effective multi-label image classification via category-aware weak supervision," in *Proceedings of the 30th ACM International Conference on Multimedia*, pp. 6318–6326, 2022.
- [26] A. Vaswani, N. Shazeer, N. Parmar, J. Uszkoreit, L. Jones, A. N. Gomez, Ł. Kaiser, and I. Polosukhin, "Attention is all you need," *Proceedings of NIPS*, vol. 30, 2017.
- [27] T.-Y. Lin, P. Goyal, R. Girshick, K. He, and P. Dollár, "Focal loss for dense object detection," in *Proceedings of ICCV*, pp. 2980–2988, 2017.
- [28] Y. Huang, J. Qi, X. Wang, and Z. Lin, "Asymmetric polynomial loss for multi-label classification," in *Proceedings of ICASSP*, pp. 1–5, 2023.
- [29] K. Wu, H. Peng, M. Chen, J. Fu, and H. Chao, "Rethinking and improving relative position encoding for vision transformer," in *Proceedings of ICCV*, pp. 10033–10041, 2021.
- [30] J. Lanchantin, T. Wang, V. Ordonez, and Y. Qi, "General multi-label image classification with transformers," in *Proceedings of CVPR*, pp. 16478–16488, 2021.
- [31] S. Woo, S. Debnath, R. Hu, X. Chen, Z. Liu, I. S. Kweon, and S. Xie, "Convnext v2: Co-designing and scaling convnets with masked autoencoders," in *Proceedings of CVPR*, pp. 16133–16142, 2023.
- [32] Z. Liu, Y. Lin, Y. Cao, H. Hu, Y. Wei, Z. Zhang, S. Lin, and B. Guo, "Swin transformer: Hierarchical vision transformer using shifted windows," in *Proceedings of ICCV*, pp. 10012–10022, 2021.
- [33] T.-Y. Lin, M. Maire, S. Belongie, J. Hays, P. Perona, D. Ramanan, P. Dollár, and C. L. Zitnick, "Microsoft coco: Common objects in context," in *Proceedings of ECCV*, pp. 740–755, 2014.
- [34] M. Everingham, S. A. Eslami, L. Van Gool, C. K. Williams, J. Winn, and A. Zisserman, "The pascal visual object classes challenge: A retrospective," *International Journal of Computer Vision*, vol. 111, pp. 98–136, 2015.
- [35] T. Ridnik, H. Lawen, A. Noy, E. Ben Baruch, G. Sharir, and I. Friedman, "Tresnet: High performance gpu-dedicated architecture," in *Proceedings of WACV*, pp. 1400–1409, 2021.
- [36] Z.-M. Chen, X.-S. Wei, X. Jin, and Y. Guo, "Multi-label image recognition with joint class-aware map disentangling and label correlation embedding," in *Proceedings of ICME*, pp. 622–627, 2019.